

# RING CURRENT DYNAMICS DURING THE 13–18 JULY 2000 STORM PERIOD

V. K. JORDANOVA<sup>1</sup>, R. M. THORNE<sup>2</sup>, C. J. FARRUGIA<sup>1</sup>, Y. DOTAN<sup>2</sup>,  
J. F. FENNELL<sup>3</sup>, M. F. THOMSEN<sup>4</sup>, G. D. REEVES<sup>4</sup> and D. J. MCCOMAS<sup>5</sup>

<sup>1</sup>*Space Science Center, University of New Hampshire, Durham, NH 03824, U.S.A.*  
(e-mail: vania.jordanova@unh.edu)

<sup>2</sup>*Department of Atmospheric Sciences, UCLA, Los Angeles, CA 90095, U.S.A.*

<sup>3</sup>*Aerospace Corporation, Los Angeles, CA 90009, U.S.A.*

<sup>4</sup>*Los Alamos National Laboratory, Los Alamos, NM 87545, U.S.A.*

<sup>5</sup>*Southwest Research Institute, San Antonio, TX 78228, U.S.A.*

(Accepted 11 June 2001)

**Abstract.** We study the development of the terrestrial ring current during the time interval of 13–18 July, 2000, which consisted of two small to moderate geomagnetic storms followed by a great storm with indices  $Dst = -300$  nT and  $Kp = 9$ . This period of intense geomagnetic activity was caused by three interplanetary coronal mass ejecta (ICME) each driving interplanetary shocks, the last shock being very strong and reaching Earth at  $\sim 14$  UT on 15 July. We note that (a) the sheath region behind the third shock was characterized by  $B_z$  fluctuations of  $\sim 35$  nT peak-to-peak amplitude, and (b) the ICME contained a negative to positive  $B_z$  variation extending for about 1 day, with a  $\sim 6$ -hour long negative phase and a minimum  $B_z$  of about  $-55$  nT. Both of these interplanetary sources caused considerable geomagnetic activity ( $Kp = 8$  to  $9$ ) despite their disparity as interplanetary triggers. We used our global ring current-atmosphere interaction model with initial and boundary conditions inferred from measurements from the hot plasma instruments on the *Polar* spacecraft and the geosynchronous Los Alamos satellites, and simulated the time evolution of  $H^+$ ,  $O^+$ , and  $He^+$  ring current ion distributions. We found that the  $O^+$  content of the ring current increased after each shock and reached maximum values of  $\sim 60\%$  near minimum  $Dst$  of the great storm. We calculated the growth rate of electromagnetic ion cyclotron waves considering for the first time wave excitation at frequencies below  $O^+$  gyrofrequency. We found that the wave gain of  $O^+$  band waves is greater and is located at larger  $L$  shells than that of the  $He^+$  band waves during this storm interval. Isotropic pitch angle distributions indicating strong plasma wave scattering were observed by the imaging proton sensor (IPS) on *Polar* at the locations of maximum predicted wave gain, in good agreement with model simulations.

## 1. Introduction

Understanding the intensity and temporal evolution of geomagnetic storms and how these relate to various interplanetary conditions is a centerpiece of space science research and NASA's Sun–Earth Connection program. The ring current represents the essential element of all geomagnetic storms; its intensification causes a sharp decrease of the horizontal component of the magnetic field measured at Earth during the main phase of the storm which is usually identified with a  $Dst$  index. During the recovery phase of the storm the ring current decays through various



loss mechanisms and the magnetic field at Earth returns to normal conditions. The energy injected from the solar wind into the ring current is subsequently transferred to the plasmasphere and upper atmosphere. The terrestrial ring current consists mostly of energetic  $H^+$  and  $O^+$  ions (e.g., Daglis, 1997) with energies between 1 and 300 keV. Some minor components of the ring current are  $He^+$ ,  $He^{++}$ , and  $C^+$  ions and electrons. The two sources of magnetospheric plasma are the solar wind and the terrestrial ionosphere and are highly variable with geomagnetic and solar activity (e.g., Yau *et al.*, 1985).

In this paper we study the global response of the ring current to the 14 July 2000 (Bastille Day) solar event. We discuss the interplanetary conditions monitored by the instruments on the ACE spacecraft which gave rise to this extremely active geomagnetic period. We simulate ring current development using our kinetic drift-loss model and data from the instruments on *Polar* and *Los Alamos National Laboratory* (LANL) spacecraft. The loss processes along ion drift paths included in our model are charge exchange, Coulomb collisions, and ion precipitation. We calculate the wave growth of electromagnetic ion cyclotron (EMIC) waves considering, in addition to previous studies, wave excitation not only in the frequency range between the  $He^+$  and  $O^+$  gyrofrequencies, but also at frequencies below the  $O^+$  gyrofrequency. Scattering by plasma waves is an important mechanism for ion precipitation (Cornwall, Coroniti, and Thorne, 1970) and may contribute to the early recovery phase of the storm. We thus look at ion precipitation data from the imaging proton sensor (IPS) on *Polar* for evidence of strong diffusion.

## 2. Observations

Interplanetary data from ACE in orbit near the L1 Lagrangian point are shown in Figure 1 for the period 13 to 18 July 2000 (see also Smith *et al.*, 2001). From top to bottom the panels show the GSM components of the magnetic field, the total field, the plasma proton density, temperature, bulk speed, dynamic pressure and epsilon parameter calculated after Perreault and Akasofu (1978). Three interplanetary shocks are evident at approximately 9 UT 13 July (S1), 15 UT 14 July (S2), and 14 UT 15 July (S3). We shall show that many parameters relating to geomagnetic effects of this extraordinary configuration are organized by this sequence of interplanetary shocks at about 1-day separation each. Behind the fast forward strong shock S3 is an approximately 5-hour region exhibiting large amplitude, compressive field fluctuations. Behind this region, from about 20 UT, 15 July to about the end of 16 July is a region where (a) the magnetic field is strongly enhanced attaining extreme values of  $\sim 60$  nT, (b) compared with adjacent values it has low variance, (c) the field vector executes a large rotation ( $B_z$  amplitude  $\sim 80$  nT) from south to north, and (d) the proton temperature is low. The dot-dashed line in panel 6 shows the temperature expected for normal solar wind expansion

## RING CURRENT DYNAMICS: JULY 13-18, 2000

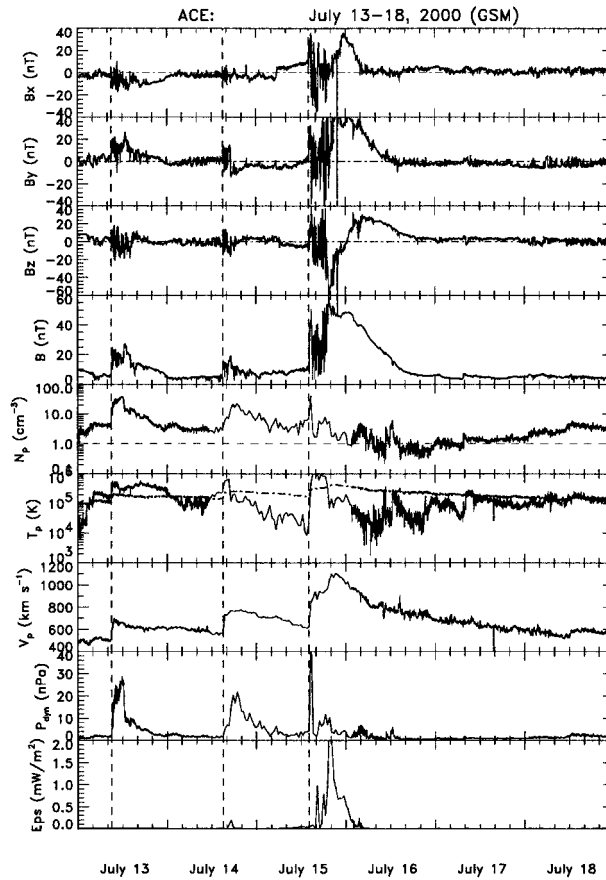


Figure 1. Interplanetary magnetic field (IMF) and plasma (proton) data from ACE on 13–18 July 2000. The vertical guidelines indicate the three interplanetary shocks S1, S2, and S3.

(Lopez, 1987). We thus identify this period as an interplanetary magnetic cloud (Burlaga *et al.*, 1981).

The dynamic pressure  $P_{\text{dyn}}$ , calculated using proton data, shows three enhancements occurring just behind each shock and has otherwise low to normal values. It follows that magnetopause current corrections to the  $Dst$  index ( $\sim \sqrt{P_{\text{dyn}}}$ ) are small (see Figure 2). At the trailing edge of the cloud on 16 July there is an interval of low-density ( $N_p < 1 \text{ cm}^{-3}$ ) discussed by Farrugia *et al.* (2000). Low-density solar wind intervals have been related to different interplanetary configurations (e.g., Richardson *et al.*, 2000). In this case, it is related to an ejection. The last panel shows the epsilon parameter, which gives the fraction of the Poynting flux through the dayside magnetopause calculated in the Perreault and Akasofu (1978) formulation. It may be interpreted as the electromagnetic power the interplanetary configuration inputs to the magnetosphere, and is dominated by a large increase

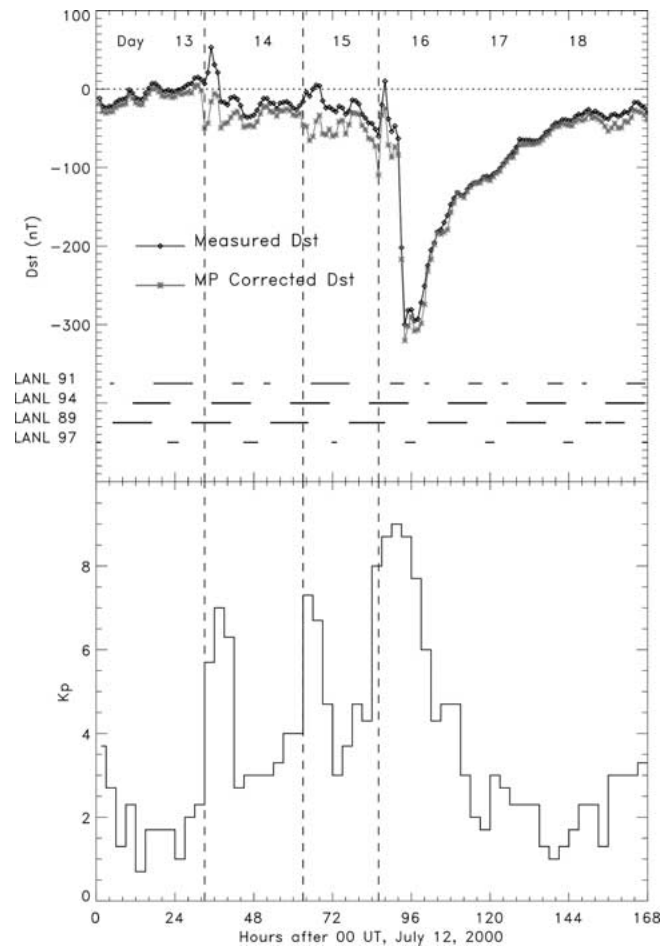


Figure 2. Top: measured (diamonds) and pressure-corrected (stars) *Dst* index. Bottom: *Kp* geomagnetic index during 12–18 July 2000. The periods when the LANL spacecraft were on the nightside are indicated by horizontal lines.

starting at shock S3, maximizing at min  $B_z$  inside the ejection and tapering off to low values as the field rotates northward.

The *Kp* index shows 3 major peaks of geomagnetic activity of progressively increasing strength (Figure 2, bottom). Each of these starts at the three shocks: S1, S2, S3, indicated with vertical guidelines. The most pronounced and strongest *Kp* disturbance corresponds to the sheath and the magnetic cloud following it on 15–16 July. At its peak  $Kp = 9$ , and, we note that the oscillating  $B_z$  field in the sheath produced comparable *Kp* activity to the continuous and large  $B_z$  activity in the magnetic cloud. Low *Kp* values ( $Kp \approx 2$ ) are reached late on 16 July when the low density interval is observed and the magnetic field is pointing northward. The measured *Dst* index (diamonds) and the *Dst* index corrected (stars) for magnetopause

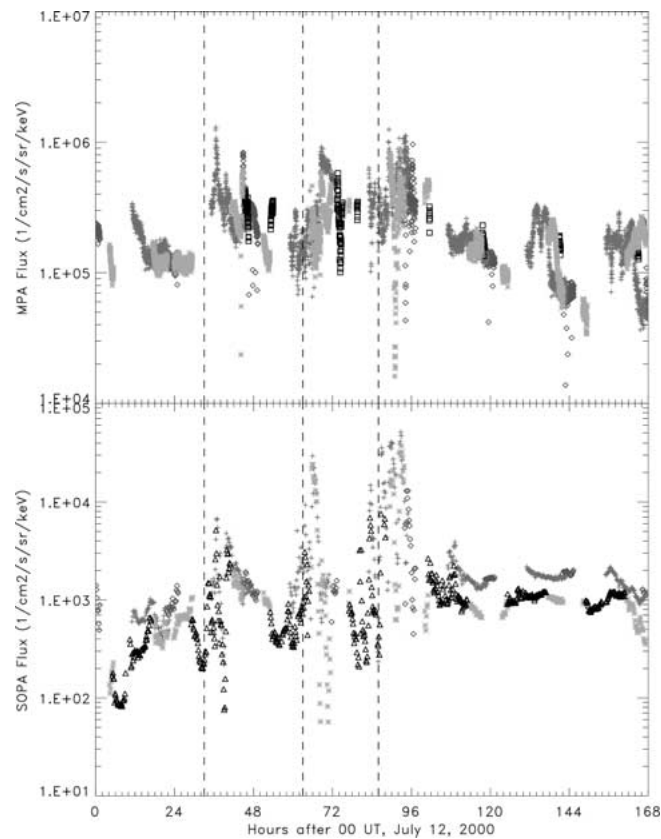


Figure 3. Ion fluxes at geosynchronous orbit during 12–18 July 2000, (top) from the 10-keV energy channel of the MPA instrument and (bottom) from the 140-keV energy channel of the SOPA instrument on LANL spacecraft (triangles, LANL 89; squares, LANL 90; stars, LANL 91; pluses, LANL 94; diamonds, LANL 97). The three interplanetary shocks are indicated with vertical guidelines.

currents (after Burton, McPherron, and Russell, 1975) are shown in the top panel of Figure 2. The pressure-corrected  $Dst$  also reflects the 3 depositions of solar wind energy at the shocks, however, the respective amplitudes of the disturbances are not the same as measured by  $Kp$ . There are minor to moderate  $Dst$  depressions during the intervals following shocks S1 and S2, but a very large decrease to values of about  $-300$  nT at the arrival of the magnetic cloud. Note the smooth  $Dst$  recovery during 16–17 July, which follows a similar trend in the  $Kp$  during this interval.

Figure 3 displays spin-averaged fluxes from the magnetospheric plasma analyzer (MPA) and synchronous orbit particle analyzer (SOPA) on the LANL geosynchronous satellites. The ion fluxes were measured when the LANL satellites were on the nightside between magnetic local time (MLT) 18 and 06. The nightside data coverage is very satisfactory throughout the investigated period (see also Figure 2). The flux level at 10-keV energy (Figure 3, top) lies between  $10^5$  and  $10^6$   $\text{cm}^{-2} \text{s}^{-1} \text{sr}^{-1} \text{keV}^{-1}$ , while that of the 140-keV energy (Figure 3, bottom)

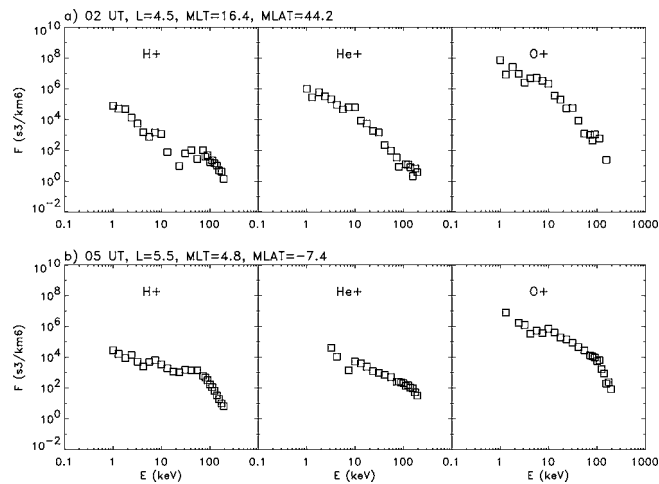


Figure 4. Measured  $H^+$ ,  $He^+$ , and  $O^+$  distribution functions from the MICS instrument on *Polar* spacecraft (a) at 02 UT, and (b) at 05 UT, 13 July.

is about  $10^3 \text{ cm}^{-2} \text{ s}^{-1} \text{ sr}^{-1} \text{ keV}^{-1}$ . Intensifications of the fluxes are observed in both energy channels after each of the three shocks. We use these data as time-dependent boundary conditions in our model to simulate particle injections from the magnetotail.

Energetic electron and ion spectra during 13–18 July 2000, at geocentric distances smaller than geosynchronous are provided by the particle instruments on *Polar*. The Global Geospace Mission spacecraft (GGS) *Polar* followed an orbit nearly along the dawn-dusk meridian during this storm period. The distribution functions of the three major ring current ion species  $H^+$ ,  $He^+$ , and  $O^+$  obtained from the magnetospheric ion composition spectrometer (MICS) on *Polar* during the quiet day of 13 July are shown at different  $L$  shells and magnetic latitudes in Figure 4 for  $MLT = 16.4$  and  $MLT = 4.8$  hours. The energy range of the MICS instrument is from 1 keV up to  $\sim 200$  keV. These data are used in our model as initial conditions.

### 3. Ring Current Model

We investigate the development of the ring current ion population during the July 2000 (Bastille Day) event employing our global drift-loss model. The model has been described in detail previously (Jordanova *et al.*, 1996, 2001) and therefore only a brief summary is presented here. The model solves the bounce-averaged kinetic equation for the distribution function  $F$  of charged particles:

$$\begin{aligned} \frac{\partial F}{\partial t} + \frac{1}{R_0^2} \frac{\partial}{\partial R_0} \left( R_0^2 \left\langle \frac{dR_0}{dt} \right\rangle F \right) + \frac{\partial}{\partial \varphi} \left( \left\langle \frac{d\varphi}{dt} \right\rangle F \right) + \frac{1}{\sqrt{E}} \frac{\partial}{\partial E} \left( \sqrt{E} \left\langle \frac{dE}{dt} \right\rangle F \right) + \\ + \frac{1}{h(\mu_0)\mu_0} \frac{\partial}{\partial \mu_0} \left( h(\mu_0)\mu_0 \left\langle \frac{d\mu_0}{dt} \right\rangle F \right) = \left\langle \left( \frac{\partial F}{\partial t} \right)_{\text{loss}} \right\rangle. \end{aligned} \quad (1)$$

We consider a region in the equatorial plane spanning radial distances  $R_0$  from  $2 R_E$  to  $6.5 R_E$  and all magnetic local times, and  $H^+$ ,  $O^+$ , and  $He^+$  particles with kinetic energy  $E$  from 100 eV to 400 keV, and equatorial pitch angle  $\alpha_0$  from  $0^\circ$  to  $90^\circ$ , where  $\mu_0 = \cos(\alpha_0)$ . The brackets  $\langle \rangle$  denote averaging between the mirror points. The function  $h(\mu_0) = S_B/2R_0$ , where  $S_B$  is the half-bounce path length.

The loss term on the right-hand side includes contributions from charge exchange with geocoronal hydrogen, Coulomb collisions with thermal plasma, wave-particle interactions, and absorption of ring current particles at low altitude in the atmosphere. The loss cone is from  $0^\circ$  to  $\alpha_{oc}$ , where  $\alpha_{oc}$  corresponds to a 200 km mirror altitude in the atmosphere. To calculate losses due to Coulomb collisions, our model is coupled with the time-dependent plasmasphere model of Rasmussen, Guiter, and Thomas (1993) which calculates electron densities in the equatorial plane. A thermal ion composition ratio of 77%  $H^+$ , 20%  $He^+$  and 3%  $O^+$  is used. The geocoronal hydrogen densities used to calculate losses due to charge exchange are obtained from the model of Rairden, Frank, and Craven (1986).

The left-hand side of Equation (1) describes adiabatic drifts of ring current ions in time-dependent magnetospheric electric and magnetic fields. In the present study we use a Volland-Stern type semi-empirical potential model which consists of a convection potential

$$U_{\text{conv}} = \frac{U(t)}{2} \left( \frac{L}{L^*} \right)^\gamma \sin \varphi = AR_0^\gamma \sin \varphi, \quad (2)$$

where  $\varphi$  is the magnetic local time in degrees with midnight at  $0^\circ$  and  $L^* = 8.5$ , and a co-rotation potential

$$U_{\text{cor}} = -C/R_0, \quad (3)$$

where  $C = 1.44 \times 10^{-2} R_E^2 \text{ V m}^{-1}$ . For the value of the parameter  $A$  as a function of  $Kp$  we use the expression determined empirically for  $\gamma = 2$  by Maynard and Chen (1975). The temporal evolution of the polar cap potential model  $U(t)$  during the investigated storm period is shown in Figure 5 (top). The magnetic field of the Earth is approximated by a three-dimensional dipole field. The magnetospheric inflow on the nightside is modeled after geosynchronous data (see Figure 3). Losses through the dayside magnetopause are taken into account, allowing free outflow of ring current particles from the dayside boundaries.

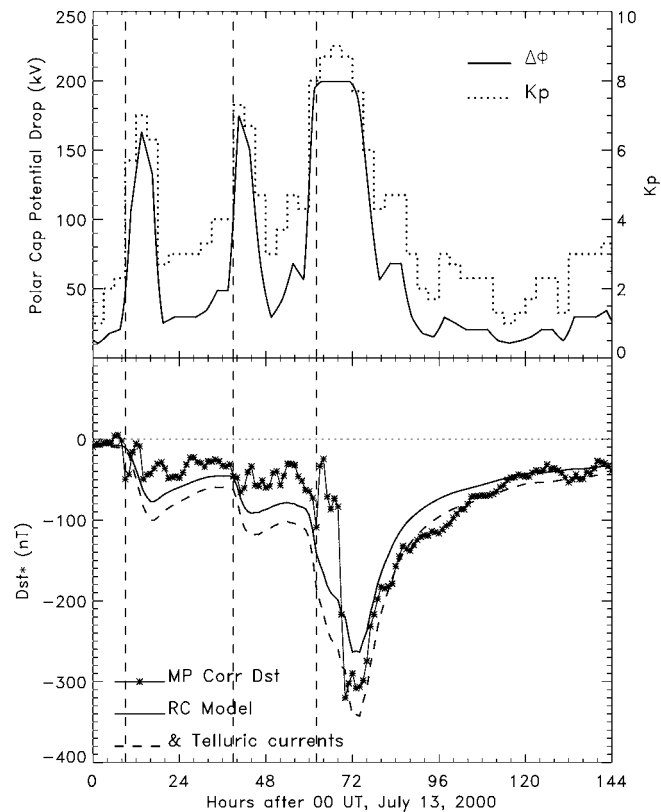


Figure 5. Top: polar cap potential drop obtained with the Volland–Stern model (solid line) and  $Kp$  index (dotted line). Bottom: pressure-corrected  $Dst^*$  index (starred line) and modeled  $Dst^*$  (solid line). The dashed line includes contribution from currents induced in the solid Earth. The UT of the three interplanetary shocks are indicated with vertical guidelines.

#### 4. Results

We simulate the evolution of  $H^+$ ,  $O^+$ , and  $He^+$  ring current ion distributions, starting our numerical computation at 00 UT, 13 July, representing the pre-storm quiet time. In this initial study we consider losses due to charge exchange, Coulomb collisions, and atmospheric collisions along ion drift paths. Scattering by plasma waves requires careful investigation, mostly because of the difficulty of estimating the wave spectrum, and will be considered in future extensions of this work. We calculate the total energy content of the ring current as the storms evolve and use the relation derived by Dessler and Parker (1959) and generalized by Skopke (1966) to compute the ring current contribution to the  $Dst$  index. The model results are plotted in Figure 5 (bottom) with a solid line. The dashed line is obtained after adding the contribution of currents induced in the solid Earth to modeled  $Dst$ . The measured  $Dst$  data have been corrected for magnetopause currents and are shown with a starred line for comparison.

The large-scale magnetospheric electric field is an important mechanism for ring current formation transporting ions earthward, energizing them, and increasing the preexisting ring current population. Three enhancements in the polar cap potential drop are predicted during 13–18 July (Figure 5, top) starting at each shock arrival. The maximum values progressively increase and the polar cap potential drop reaches saturation of  $\sim 200$  kV after the third shock. The ring current (i.e., the  $|Dst^*|$  index) follows the changes of the convection potential, gradually increasing during the main phases of the storms and reaching maximum about 3 to 4 hours after  $U(t)$  maximum, then decreasing and reaching minimum at the end of the model recovery phases. Extreme values are reached during the last, largest storm. Comparing with the pressure-corrected  $Dst^*$  values, the model reproduces reasonably well the main trends of ring current buildup and decay during this storm period. The remaining discrepancies may be due to the simplified Volland-Stern type electric field model we use and will be investigated in further studies.

In Figure 6 (top) we show the globally averaged  $O^+$  energy density percentage obtained from our model during 13–18 July 2000 (solid line). The  $O^+$  density percentage at geosynchronous orbit from the statistical study of Young, Balsiger, and Geiss (1982) is shown with a dash-dot line. The Young *et al.* values are applied at the nightside boundary of our model to determine the  $O^+$  content since the LANL instruments do not provide ion composition information. We find that during this solar-max storm period  $O^+$  content exceeded 50% behind each of the three shocks and did not drop below 45% during the passage of the three shock-ejecta system (up to hour  $\sim 104$ ). Near  $Dst$  minima  $O^+$  became the dominant ion and during the great storm it contributed  $\sim 60\%$  of the total ion energy density for about 10 hours. This is in agreement with CRRES (Combined Release and Radiation Effects Satellite) observations during a storm of comparable strength which occurred on 24 March 1991 (Daglis, 1997). Figure 6 displays as well dial plots of the energy density of the major ring current ion species  $H^+$ ,  $He^+$ , and  $O^+$  as a function of radial distance in the equatorial plane and MLT at hour 36 (a), 72 (b), and 96 (c) after 00 UT, 13 July. Pronounced ring current asymmetry is evident during the main phase of the great storm (hour 72), with energy density maximizing near the dusk sector for all ions. As noted above,  $O^+$  is the dominant ion at this time and its energy density reaches the largest values. Such ring current asymmetry is not present during less disturbed times shown in Figure 6 at hour 36 (a) and hour 96 (c).

To investigate the excitation of plasma waves by the anisotropic ring current ion populations, we calculate the equatorial convective growth rates of EMIC waves (Pc 1-2) as a function of  $L$  shell and MLT with storm evolution. The wave gain obtained after integrating the growth rates along field-aligned wave paths is shown in Figure 7 for various universal times after 00 UT, 13 July. In addition to previous studies we consider wave excitation not only in the frequency range between the  $He^+$  and  $O^+$  gyrofrequencies ( $He^+$  band waves shown in the left panel), but also in the frequency range below  $O^+$  gyrofrequency ( $O^+$  band waves shown in the right panel). Thorne and Horne (1997) have shown that increased  $O^+$  content favors

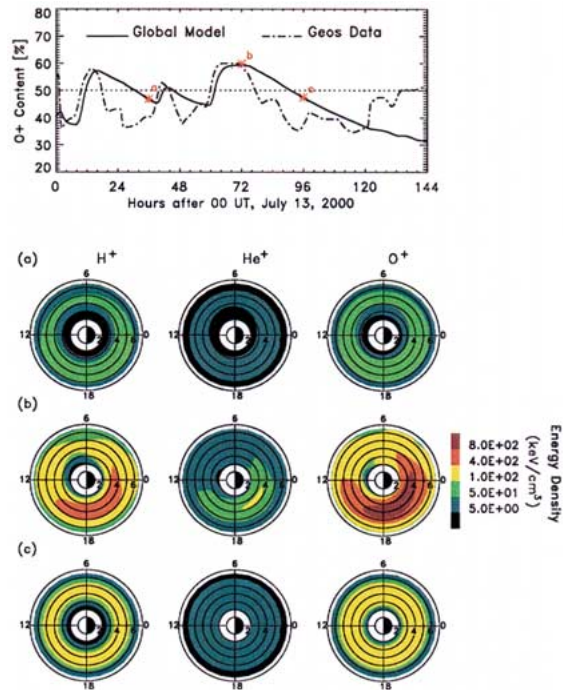


Figure 6. Top: content of ring current  $O^+$ . Bottom:  $H^+$ ,  $He^+$ , and  $O^+$  ring current ion energy density at selected hours indicated with (a), (b), and (c) in the top panel.

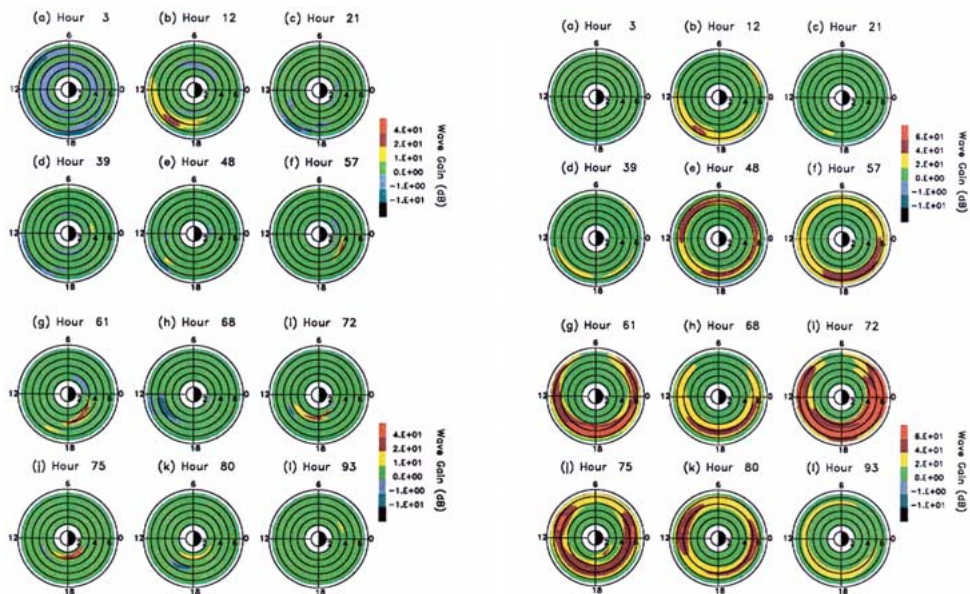


Figure 7. Wave gain of  $He^+$  (left) and  $O^+$  (right) band of EMIC waves at hours after 00 UT, 13 July.

the generation of waves below the  $O^+$  gyrofrequency and damps waves above it. As we see, during this storm period the wave gain of the  $O^+$  band waves exceeds the magnitude of the  $He^+$  band wave gain (note the difference in the color bars). The most unstable regions form after intensification of the ring current, i.e., near  $Dst$  minimum, and are located in the post noon to midnight local time sector. The  $He^+$  band waves are usually excited at lower  $L$  shells than the  $O^+$  band waves. Consistent with this, EMIC waves near the  $O^+$  gyrofrequency were observed by ISEE 1 and 2 between  $L = 5.8$  and  $7.6$  in the dusk sector (Fraser *et al.*, 1992). The most intense waves had amplitudes  $B_w = 8$  nT and were observed in the outer plasmasphere. More recently, waves below the  $O^+$  gyrofrequency were observed by the instruments on the Freja spacecraft near  $Dst$  minimum of the major geomagnetic storm in 2–8 April, 1993 (Brasys, Mursula, and Marklund, 1998).

Ring current ions are scattered into the loss cone due to resonant interactions with EMIC waves and precipitate into the atmosphere. Ion pitch angle distributions from the imaging proton sensor (IPS) of the comprehensive energetic particles and pitch angle distribution (CEPPAD) experiment on *Polar* during 15 and 16 July, 2000, are shown in Figures 8 and 9, respectively. The data are from the P4 energy channel (57.2 keV midpoint energy) for  $L = 7$  to  $L = 3$  (from top to bottom) in the dusk sector (MLT  $\sim 16$  to MLT  $\sim 18$ ). The local loss cone is identified with vertical guidelines; the upward looking loss cone (i.e., ions precipitating toward the Earth) corresponds from  $0^\circ$  to  $\sim 15^\circ$  in the northern hemisphere and from  $\sim 155^\circ$  to  $180^\circ$  in the southern. The pitch angle distributions are isotropic across the upward looking loss cone at  $L = 6$  and  $L = 7$  at  $\sim 9$  UT, 15 July (hour 57) and at  $L = 4$  to  $L = 7$  at  $\sim 3$  UT, 16 July (hour 75). This is indicative of strong diffusion scattering. Comparing with the calculated EMIC wave gain at hours 57 and 75 (Figure 7), these locations coincide with the regions of intense  $O^+$  band waves excitation. Partially filled loss cones, indicating moderate diffusion are observed at lower  $L$  shells and at 21 UT, 16 July (hour 93). As we see from Figure 7, the wave gain of the EMIC waves has smaller magnitude at these times and locations. Empty loss cones indicating no diffusion were observed by the IPS instrument during less geomagnetically active periods on 13 July and 17 July. Our model did not predict EMIC wave excitation at these times, in good agreement with *Polar* observations.

## 5. Summary and Conclusions

Three shocks were observed in the interplanetary medium on 13, 14, and 15 July 2000, each driven by an ejection. The third of these ejecta was a magnetic cloud where ACE observed a negative to positive  $B_z$  excursion from about  $-55$  nT to  $\sim 25$  nT, which is extreme in amplitude. In the sheath region ahead of the third ejection there were large amplitude magnetic field oscillations, which were also strongly geoeffective. Correspondingly, three bursts of magnetic activity were observed in the near-terrestrial environment, starting at the time of each shock. The

## IPS P4— 57.2KeV Pitch Angle Distribution Summary Plots, 0715, Pass1

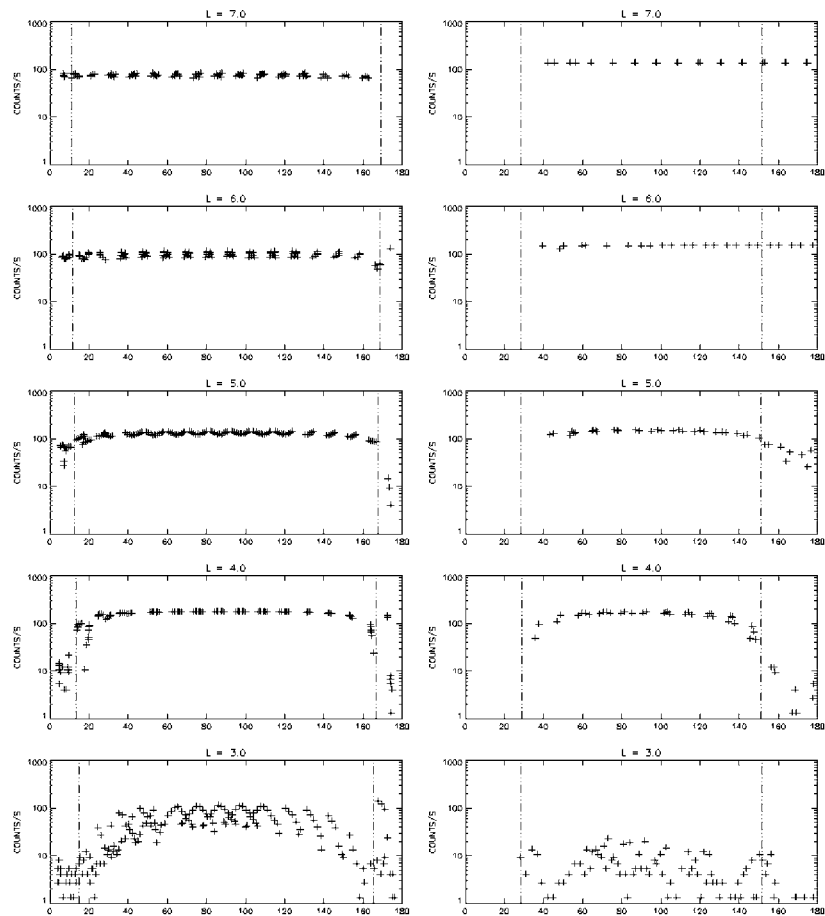


Figure 8. Ion pitch angle distributions from the IPS instrument on *Polar* from the northern (*left*) and southern (*right*) passes at  $\sim 9$  UT, 15 July 2000.

geomagnetic indices progressively increased and reached max  $Kp = 9$  and  $Dst = -300$  nT at the end of 15 July. The LANL/MPA and SOPA instruments measured energetic ion flux enhancements at geosynchronous following each interplanetary shock.

We simulated the evolution of the terrestrial ring current during this period using our global drift-loss model; *Polar*/MICS and LANL data provided the initial and boundary conditions. We found that the model reproduced reasonably well the ring current contribution to the  $Dst$  index. Three ring current injections corresponded to the interplanetary shocks, the first two causing small to moderate storms, while the third one caused a great geomagnetic storm. Ring current energy density calculations indicated a very asymmetric distribution during the main and early recovery

## IPS P4– 57.2KeV Pitch Angle Distribution Summary Plots, 0716, Pass1–2

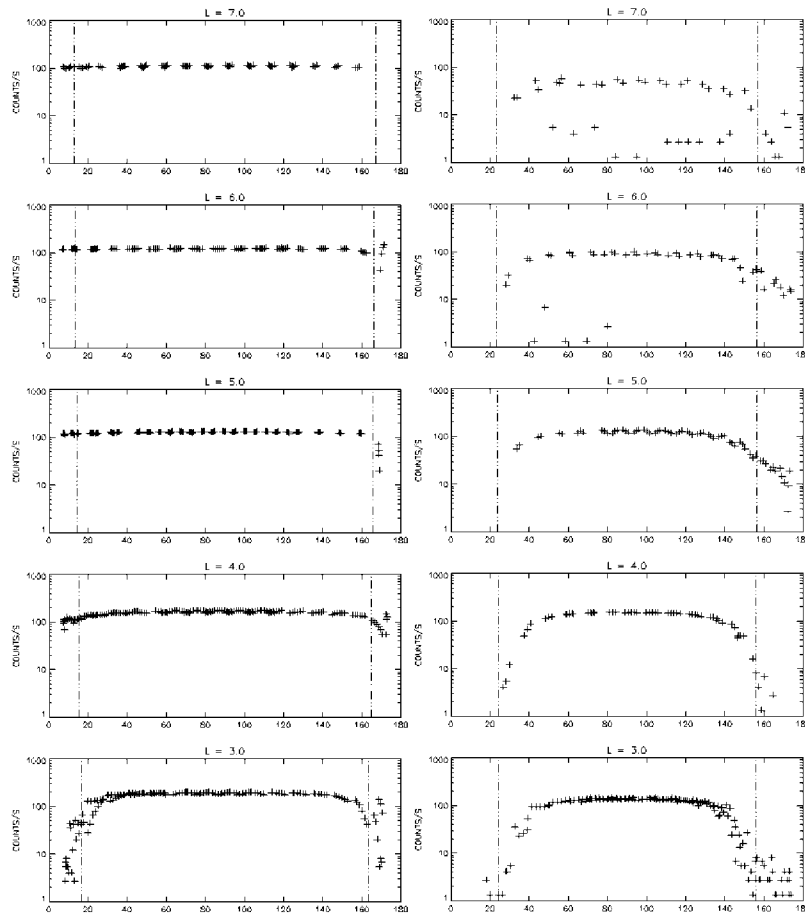


Figure 9. Ion pitch angle distributions from the IPS instrument on *Polar* from the northern pass at  $\sim 3$  UT, 16 July (left) and from the southern pass at  $\sim 21$  UT, 16 July (right).

phases of the great storm for all three ion species studied,  $H^+$ ,  $He^+$ , and  $O^+$ . It is only during the late recovery phase of the storm that the ring current became symmetric. We calculated the  $O^+$  contribution to the ring current during the storm period and found that: (a)  $O^+$  content increased significantly behind each of the three shocks, (b) during passage of the three shock-ejecta system the  $O^+$  content of the ring current did not drop below 45%, and (c) at the main phase of the great storm the ring current consisted of up to 60%  $O^+$ , in agreement with previous observational studies of storms of comparable strength.

We further developed our model to study the excitation of both  $He^+$  and  $O^+$  band EMIC waves by the hot ring current ion populations during 13–18 July 2000.

We found that the wave gain of the O<sup>+</sup> band waves exceeded the magnitude of the He<sup>+</sup> band wave gain during this intense storm period. In addition, the O<sup>+</sup> band waves were excited at larger *L* shells in the dusk local time sector. Isotropic pitch angle distributions indicative of strong diffusion scattering were observed by the *Polar/IPS* instrument within the regions of large O<sup>+</sup> band waves excitation during the main and early recovery phases of the great storm. Partially filled or empty loss cones were observed at lower *L* shells and during less disturbed periods. In agreement, our model predicted smaller EMIC wave gain at these times. In order to accurately predict the precipitating ion flux levels, the calculated wave gain must be converted to a realistic wave amplitude. For this purpose, a comparative study of modeled wave gain with experimentally observed wave amplitudes will be performed in future extensions of this work. Quantitative comparison of calculated with observed levels of proton precipitation will be used to validate our wave amplitude model.

### Acknowledgements

Special thanks to Ruth Skoug for help with ACE plasma data analysis. This work is supported in part by NASA under grants NAG5-7804, NAG5-10883 and NAG5-2834, and NSF under grant ATM97-29021.

### References

- Braysy, T., Mursula, K., and Marklund, G.: 1998, *J. Geophys. Res.* **103**, 4145.
- Burlaga, L. F., Sittler, E., Mariani, F., and Schwenn, R.: 1981, *J. Geophys. Res.* **86**, 6673.
- Burton, R. K., McPherron, R. L., and Russell, C. T.: 1975, *J. Geophys. Res.* **80**, 4204.
- Cornwall, J. M., Coroniti, F. V., and Thorne, R. M.: 1970, *J. Geophys. Res.* **75**, 4699.
- Daglis, I. A.: 1997, in B. T. Tsurutani, W. D. Gonzalez, Y. Kamide, J. K. Arballo (eds.), *Magnetic Storms*, American Geophysical Union, Washington, p. 107.
- Dessler, A. J. and Parker, E. N.: 1959, *J. Geophys. Res.* **64**, 2239.
- Farrugia, C. J., Matsui, H., Torbert, R. B., Scudder, J. D., Ogilvie, K. W., Fitzenreiter, R. J., Evans, D. S., McComas, D., Lepping, R. P., and Needell, J.: 2000, *Eos. Trans. AGU* **81**, 1016.
- Fraser, B. J., Samson, J. C., Hu, Y. D., McPherron, R. L., and Russell, C. T.: 1992, *J. Geophys. Res.* **97**, 3063.
- Jordanova, V. K., Kistler, L. M., Kozyra, J. U., Khazanov, G. V., and Nagy, A. F.: 1996, *J. Geophys. Res.* **101**, 111.
- Jordanova, V. K., Farrugia, C. J., Thorne, R. M., Khazanov, G. V., Reeves, G. D., and Thomsen, M. F.: 2001, *J. Geophys. Res.* **106**, 7.
- Lopez, R. E.: 1987, *J. Geophys. Res.* **92**, 11189.
- Maynard, N. C. and Chen, A. J.: 1975, *J. Geophys. Res.* **80**, 1009.
- Perreault, P. and Akasofu, S.-I.: 1978, *Geophys. J.R. Astron. Soc.* **54**, 547.
- Rairden, R. L., Frank, L. A., and Craven, J. D.: 1986, *J. Geophys. Res.* **91**, 13613.
- Rasmussen, C. E., Guitter, S. M., and Thomas, S. G.: 1993, *Planetary Space Sci.* **41**, 35.
- Richardson, I. G., Berdichevsky, D., Desch, M. D., and Farrugia, C. J.: 2000, *Geophys. Res. Lett.* **27**, 3761.

- Sckopke, N.: 1966, *J. Geophys. Res.* **71**, 3125.
- Smith, C. W., Ness, N. F., Burlaga, L. F., Skoug, R. M., McComas, D. J., Zurbuchen, T. H., Gloeckler, G., Haggerty, D. K., Gold, R. F., Desai, M. I., Mason, G. M., Mazur, J. E., Dwyer, J. R., Popecki, M. A., Moebius, E., Cohen, C. M. S., and Leske, R. A.: 2001, *Solar Phys.*, this issue.
- Thorne, R. M. and Horne, R. B.: 1997, *J. Geophys. Res.* **102**, 14141.
- Yau, A. W., Shelley, E. G., Peterson, W. K., and Lenchyshyn, L.: 1985, *J. Geophys. Res.* **90**, 8471.
- Young, D. T., Balsiger, H., and Geiss, J.: 1982, *J. Geophys. Res.* **87**, 9077.